Biomedicine & Pharmacotherapy 199 (2026) 119433

Contents lists available at ScienceDirect

Biomedicine & Pharmacotherapy

journal homepage: www.elsevier.com/locate/biopha

Dual inhibition of PP2A and WEE1 induces apoptosis and mitotic catastrophe in cancer cells

Al-Hassan M. Mustafa [a,b,1], Alexandra Nguyen [a,1], Sophie Kreissig [c], Yanira Zeyn [d], Yesim Melisa Gürbüzoglu [a], Stefan Stoldt [d], Matthias Bros [e], Markus P. Radsak [f,g], Walburgis Brenner [h], Linping Chen-Wichmann [c], Christian Wichmann [c], Oliver H. Krämer [a,*]

[a] Institute of Toxicology, University Medical Center of Johannes Gutenberg University Mainz, Mainz 55131, Germany
[b] Department of Zoology, Faculty of Science, Aswan University, Aswan, Egypt
[c] Division of Transfusion Medicine, Cell Therapeutics and Haemostaseology, University Hospital, LMU Munich, Munich, Germany
[d] Imaging Core Facility, Cell Biology Unit, University Medical Center of Johannes Gutenberg University Mainz, Mainz 55131, Germany
[e] Department of Dermatology, University Medical Center of Johannes Gutenberg University Mainz, Mainz 55131, Germany
[f] present address: Department of Hematology and Oncology, Donau-Isar Hospitals, Deggendorf, Germany
[g] Department of Hematology and Medical Oncology, University Medical Center of Johannes Gutenberg University, Mainz, Germany, Donau-Isar Hospitals, Deggendorf, Germany
[h] Clinic for Obstetrics and women's health, University Medical Center, Mainz 55131, Germany

ARTICLE INFO

Keywords:
Cancer
DNA damage
Drug interaction
PP2A
Primaries
WEE1

ABSTRACT

The serine/threonine phosphatase-2 (PP2A) controls mitogen-associated signaling and DNA replication. The WEE1 protein tyrosine kinase controls S phase progression and G2/M phase transition. Databases disclose that the levels of PP2A and WEE1 are associated with poor prognosis of leukemic patients (p = 0,0017/0,025; n = 54–163). We applied advanced, clinically used drugs that block PP2A and WEE1 to human cultured leukemia cells, primary pre-leukemic and chronic myeloid leukemia cells, and pancreatic ductal adenocarcinoma cells. Combined application of the drugs depleted cells in all cell cycle phases, synergistically triggered apoptosis, and evoked the induction of DNA stress foci and mitotic catastrophe. In 93 lymphoid, 40 myeloid, and 47 pancreatic cancer cells, genetic depletion of PP2A-Cα and WEE1 stalls the proliferation of most cells. Unlike cancer cells, normal human immune cells are not killed upon inhibition of PP2A and WEE1. This is linked to higher expression of PP2A and WEE1 in chronic myeloid (n = 274), acute myeloid (n = 1858) and acute lymphoblastic leukemia cells (n = 1817) than in normal blood cells. These data suggest that pharmacological modulators of serine/threonine and tyrosine signaling allow targeted chemotherapy.

1. Introduction

Protein phosphorylation modulates key physiological processes and is frequently dysregulated in tumors [1]. Kinases and phosphatases control protein phosphorylation antagonistically. Kinases consume ATP and phosphatases cleave phosphate groups hydrolytically. Kinases are the best characterized anti-cancer targets and phosphatases increasingly turn in the focus of cancer research [2]. There are several protein phosphatase families. The serine/threonine phosphatase-2A (PP2A) consists of the catalytically active subunit PP2A-C that forms complexes with the scaffolding subunit PP2A-A and regulatory PP2A-B-type subunits. The diverse, regulatory subunits determine the substrate specificity and the localization of catalytically active PP2A-A/C complexes in vivo [3–5]. PP2A complexes regulate multiple cellular processes including DNA repair, RNA splicing, apoptosis, autophagy, protein aggregation, and cell proliferation in healthy and transformed cells [2, 6–9]. Accordingly, dysregulation of PP2A and its various subunits is associated with severe diseases, such as Alzheimer disease,

* Corresponding author.
E-mail addresses: alabdeen@uni-mainz.de (A.-H.M. Mustafa), Phuc.nhien@hotmail.de (A. Nguyen), Sophie.Kreissig@med.uni-muenchen.de (S. Kreissig), yanira.zeyn@uni-mainz.de (Y. Zeyn), yguerbue@students.uni-mainz.de (Y.M. Gürbüzoglu), stoldtst@uni-mainz.de (S. Stoldt), mbros@uni-mainz.de (M. Bros), radsak@uni-mainz.de (M.P. Radsak), brenner@uni-mainz.de (W. Brenner), Linping.Chen-Wichmann@med.uni-muenchen.de (L. Chen-Wichmann), Christian.Wichmann@med.uni-muenchen.de (C. Wichmann), okraemer@uni-mainz.de (O.H. Krämer).
[1] equal first author contributions

https://doi.org/10.1016/j.biopha.2026.119433
Received 17 October 2025; Received in revised form 27 March 2026; Accepted 21 April 2026
Available online 8 May 2026

autoimmunity, and cancer. PP2A has tumor suppressive as well as oncogenic functions [2,7]. Therefore, clarifying the exact functions of PP2A complexes in specific biological systems may offer attractive targets for precise targeted therapies.

In phase I/II clinical trials, the small molecule ATP-competitive PP2A inhibitor LB-100 has produced benefits in patients with various solid and hematopoietic cancers, including lung cancer, glioblastoma, myelodysplastic syndrome (MDS), pancreatic adenocarcinoma (PDAC), and further, primary and relapsed tumors [10,11]. Recent data suggest that the small molecule PP2A inhibitor phendione promotes pro-proliferative extracellular kinase (ERK) signaling and DNA damage signaling without detectable DNA damage and without the induction of quiescence that dampens chemosensitivity in melanoma cells. In a direct comparison with LB100, this study further showed that phendione was more specific and active at lower concentrations [8]. In colon cancer cells, it was confirmed that LB100 activates pro-proliferative kinase cascades. This hyperactivation of oncogenic signaling pathways can render cells susceptible to a concomitant inhibition of the tyrosine kinase WEE1 [6]. WEE1 controls DNA replication origin firing, the supply of dNTP levels in S phase, and the activity of the mitotic CDK1/cyclin B complex that promotes G2/M phase progression [12–14]. The ATP-competitive WEE1 inhibitor adavosertib is currently the most advanced WEE1 inhibitor. Adavosertib is used in clinical studies in combination with chemotherapeutics and/or radiotherapy to eradicate various tumors. Although such treatments produced promising results, issues with toxicity limit the applicability of such therapies. More biomarkers for the usefulness and efficacy of adavosertib and its combinations remain to be identified [15,16].

We set out to define how phendione affected the survival and cell cycle progression of cultured and primary leukemic cells and PDAC cells, if additional inhibition of WEE1 augmented anti-tumor effects of phendione, and if this was specific for tumor cells.

2. Results

2.1. Phendione induces apoptosis that is linked to PP2A inhibition in leukemia cells

Using public data resources, we first estimated if the levels of PP2A were associated with the survival of leukemia patients and whether leukemia cell proliferation was dependent on PP2A. The GEPIA2 database illustrates that higher expression levels of PP2A in 54 patients with acute myeloid leukemia (AML) correlate with worse patient prognosis (Fig. 1**A**; p = 0,00017). A CRISPR-Cas9-based dataset in the cancer cell Dependency Map (DepMap) portal shows that out of 93 lymphoid and 42 myeloid cancer cell types over 80% rely on the PP2A catalytic subunit α (PP2CA) for their proliferation. The average dependency values for both leukemia cell groups are between −0.4 and −0.7 and several cell types display an absolute dependency (values at or below −1 indicate a necessary gene) (Fig. 1**B**). The cells though seem to grow independently of the PP2A catalytic subunit β (supplemental Fig. 1**A**).

This encouraged us to evaluate the responses of cultured human leukemia cells to a pharmacological inhibition of PP2A. We incubated AML cells (MV4–11), acute lymphatic leukemia cells (ALL, RS4–11), Burkitt lymphoma cells (Ramos), erythroleukemic cells (HEL), and chronic myeloid leukemia cells (CML, K562) with 0.1–1 μM phendione for 24 h. Treatment with 1 μM phendione increased the apoptotic cell fractions to 83.9% in MV4–11 cells, to 64.1% in RS4–11 cells, to 37.6% in Ramos cells, and to 49.4% in HEL cells. These values were statistically significant for early and late apoptosis induction in MV4–11, RS4–11, and Ramos cells (Fig. 1**C**). Therefore, we used these cells for further analyses.

We treated MV4–11, RS4–11, and Ramos cells with 100–300 nM phendione for 72 h. After 24 h, 100 nM phendione did not induce apoptosis significantly in these cell types (Fig. 1**C**). However, a significant number of cells accumulated in RS4–11 and Ramos cell cultures in early and late apoptosis upon treatment with 100 nM phendione for 72 h. These effects increased dose-dependently. In MV4–11 cells, 300 nM phendione caused apoptosis significantly. Total apoptosis at 300 nM dosing of phendione reached 73.6% in MV4–11 cells, 87.3% in RS4–11 cells, and 98.4% in Ramos cells (Fig. 1**D**).

Next, we used human CD34-positive MLL-ENL+ pre-leukemic cells as primary *in vitro* model. These were transduced human CD34 + cells from healthy donors with the t(11;19) *MLL-ENL* oncogene. We treated them with ethanol as solvent control, 100 nM, 500 nM, or 1 μM phendione for 24–48 h. These cells were counted and stained for annexin-V/PI to determine apoptosis and cell proliferation. We found that 500 nM phendione stalled their proliferation and that 1 μM phendione suppressed their growth significantly (Fig. 1**E**). Flow cytometry revealed that this anti-proliferative effect of phendione was due to apoptosis induction up to 63.8% after treatment with 1 μM phendione for 48 h (Fig. 1**F**).

We then assessed how phendione affected patient-derived mononuclear cells that we collected upon an unfavorable transition of CML into leukemic blast crisis (Fig. 1**G**). We treated this clinical specimen with 500 nM phendione for 24 h and 48 h. Flow cytometry demonstrated that phendione induced apoptosis significantly up to 83% in patient-derived CD34 + leukemic cells after 24 h and 48 h ex vivo (Fig. 1**H**).

To strengthen the causal relationship between phendione, PP2A on target activity, and subsequent apoptotic responses, we treated MV4–11 and RS4–11 cells with 1 μM phendione for 1 h and 3 h. We chose such early treatment periods to avoid the detection of the above-shown cell death-associated processes and altered proteasomal activities [9] and focused on the detection of well-established PP2A target proteins [3]. Flow cytometry confirmed that no apoptosis was evident in both cell types when they were exposed to 1 μM phendione for up to 3 h (Fig. 1**I**). Immunoblot analysis revealed an accumulation of phosphorylated levels of the kinases p38 and AKT1 and of the DNA replication stress-induced signaling molecules CHK1 and KRAB-associated protein-1 (KAP1) upon inhibition of PP2A. These processes occurred early and preceded any apoptotic event, as evidenced by stable levels of PARP1. Likewise, PR130 remained stable (Fig. 1**J**), which disfavors altered protein stability after such short treatment periods.

These data illustrate that PP2A is a druggable vulnerability in leukemia cells from various hematopoietic origins.

2.2. Adavosertib causes apoptosis in leukemia cells

The PP2A inhibitor LB100 and adavosertib combine favorably against colon cancer cells [6]. We analyzed the relevance of WEE1 with databases on leukemic patient survival and with experiments in cell lines. The GEPIA2 database shows that higher expression levels of WEE1 are linked to worse patient prognosis in 163 AML patients (Fig. 2**A**; p = 0,025). The DepMap portal indicates that 93 lymphoid and 42 myeloid cell types depend on WEE1. The average dependency values for both leukemia cell groups are between −2 and −3 (Fig. 2**B**).

We previously found that 500 nM adavosertib shut down WEE1 signaling [17]. Therefore, we incubated 500 nM adavosertib for 24 h and 48 h. We found that 500 nM adavosertib induced 60–80% apoptosis time-dependently in patient-derived CD34 + leukemic blasts ex vivo (Figs. 2**C**,2**D**).

These findings demonstrate that leukemia cells require WEE1 activity to grow and survive.

2.3. The combination of phendione and adavosertib causes apoptosis in leukemia cells

To elucidate if inhibitors of PP2A and WEE1 interact against leukemia cells, we determined BLISS and HSA synergy score analyses. We treated MV4–11 AML cells and RS4–11 ALL cells with a dose matrix of 0.1–1 μM phendione along with 0.1–1 μM adavosertib for 24 h and

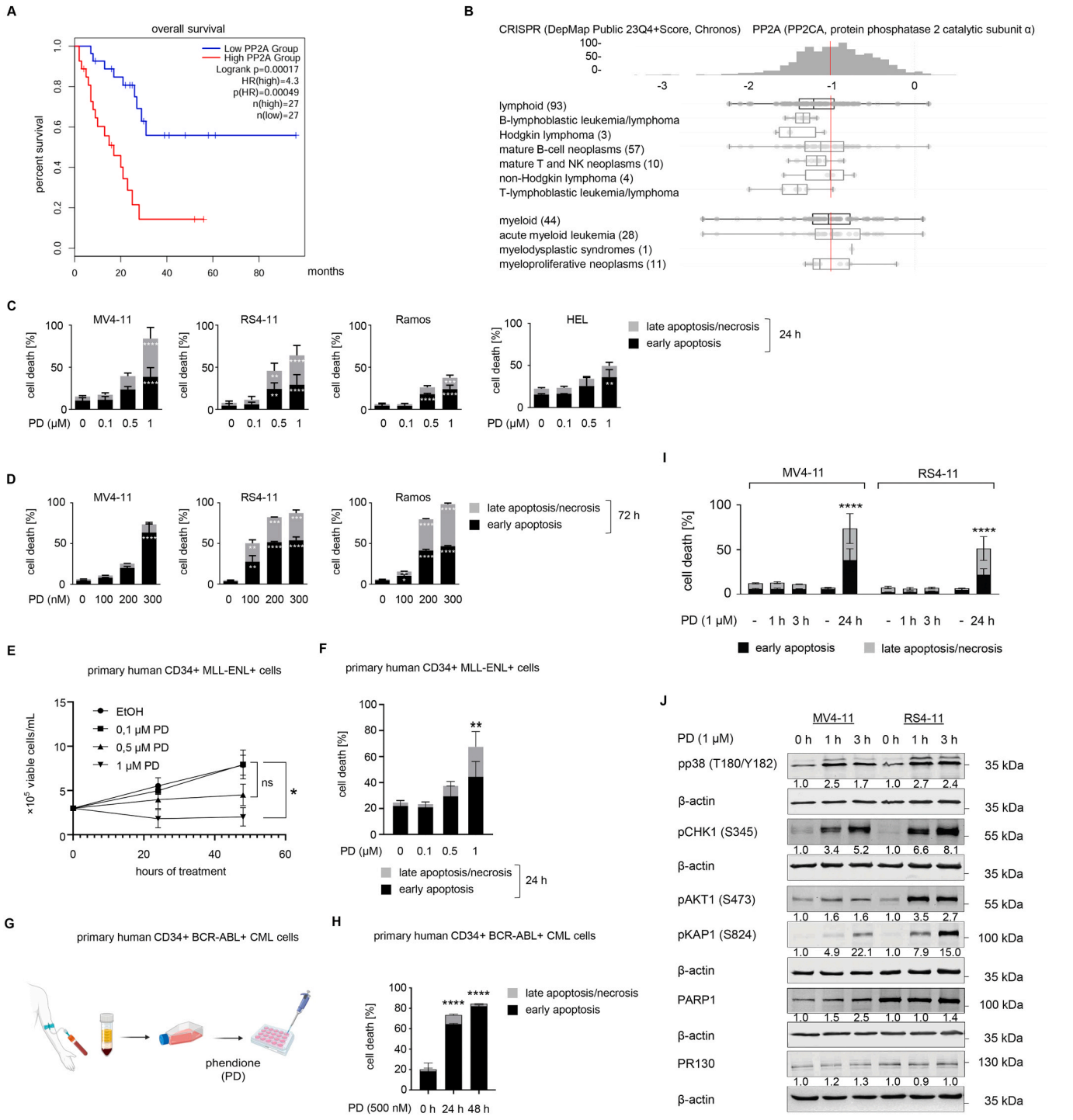

Fig. 1. Phendione induces apoptosis-associated DNA fragmentation in leukemic cells. (A) Database analyses show a link between PP2A expression levels in AML cells and disease progression of patients (cutoff 25% low and 75% high; GEPIA2 contains the TCGA and GTEx database information; GEPIA 2 (cancer-pku.cn)). (B) The DepMap database informs how a CRISPR-Cas9-based depletion of the protein phosphatase 2 catalytic subunit alpha (*PPP2CA/PP2Cα*) is a dependency factor in the shown leukemia cell types. The graph shows the dependency of all analyzed cell types (*https://depmap.org/portal/gene*). (C) The indicated cell lines were treated with 0.1–1 μM phendione (PD) for 24 h. Annexin-V/PI-stained cells were analyzed by flow cytometry. (D) MV4-11, RS4-11, and Ramos cells were treated with 100 nM, 200 nM and 300 nM and incubated for a further 72 h. The cells were then harvested, stained with annexin-V and PI, and subjected to flow cytometry. (E) Human CD34/MLL-ENL-positive cells were treated as indicated. The proliferation of viable cells was followed up to 48 h; adjusted p-value ethanol vs. 1 μM after 48 h = 0,0435; n = 3. (F) Such cells were harvested at 24 h and stained with annexin-V to determine cell death by flow cytometry. (G) Schematic diagram for the collection of primary CML cells and showing their treatment with phendione ex vivo. Mononuclear cells are collected from the arm crook, isolated by centrifugation, cultured, and treated with 500 nM phendione. (H) Primary CD34 + CML cells were treated with 500 nM phendione for 24 h and 48 h. Flow cytometry was performed to measure annexin-V/PI-positive cells; n = 3. (I) MV4-11 and RS4-11 cells were treated with 1 μM phendione for 1 h, 3 h, or 24 h, harvested, stained with annexin V/PI, and analyzed for cell death by flow cytometry; n = 3. (J) MV4-11 and RS4-11 cells were treated with 1 μM for 1 h and 3 h, harvested, lysed, and immunoblot was performed to detect the levels as well as the posttranslational modifications of indicated proteins. Data represents three independent experiments. Data are means ± SD; n = 3–4; statistical analyses were done using analysis of variance (two-way ANOVA) (* $p < 0.05$, ** $p < 0.01$, *** $p < 0.001$, **** $p < 0.0001$); numbers below blots are densitometric values divided by signals for loading control.

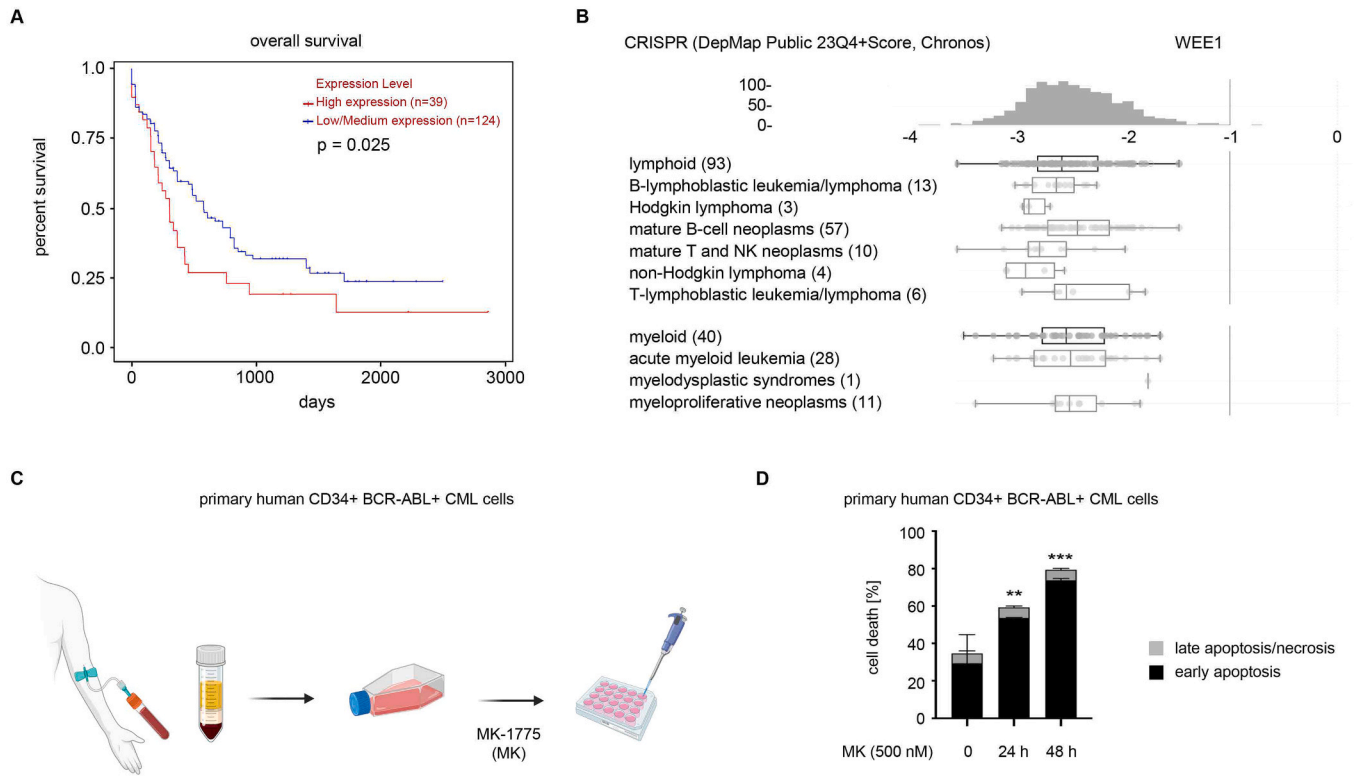

Fig. 2. WEE1 inhibition kills leukemic cells. (A) Database analyses show a link between WEE1 expression levels in AML cells and disease progression of patients (cutoff 25% low and 75% high; UALCAN database: an update to the integrated cancer data analysis platform that contains the TCGA, MET500, CPTAC and CBTTC, and GTEx database information; (https://ualcan.path.uab.edu/analysis.html)). (B) The DepMap database informs how a CRISPR-Cas9-based depletion of WEE1 is a dependency factor in the shown cell types. The graph shows the dependency of all analyzed cell types (https://depmap.org/portal/gene). (C) Schematic diagram for the collection of primary CML cells and showing their treatment with adavosertib (MK-1775) ex vivo. Mononuclear cells were isolated, cultured, and treated with 500 nM adavosertib. (D) Primary CD34 + CML cells were treated with 500 nM adavosertib (MK) for 24 h and 48 h. Cells were harvested, stained with annexin-V/PI, and analyzed for cell death by flow cytometry; n = 3; statistical analyses were done using analysis of variance (two-way ANOVA) (** $p < 0.01$, *** $p < 0.001$).

measured early and late apoptosis. In these cells, simultaneous inhibition of PP2A and WEE1 induced apoptosis synergistically, within a range between 5.052 and 12.907 (Fig. 3**A-D**).

Based on this evidence, we treated MV4–11 and RS4–11 cells with 500 nM phendione and 500 nM adavosertib. Consistent with Fig. 1**C**, adavosertib induced apoptosis significantly in MV4–11 cells and both phendione and adavosertib induced apoptosis significantly in RS4–11 cells. In both leukemia cell types, 500 nM phendione plus 500 nM adavosertib increased the fractions of cells in early apoptosis and late apoptosis/necrosis significantly. Independent of the effects of the single agents, apoptosis was potentiated when these compounds were applied together (Fig. 3**E**).

As WEE1 is a key cell cycle regulator, we consequently analyzed with flow cytometry how adavosertib and phendione affected cell cycle phase distributions of MV4–11 and RS4–11 cells after 24 h. In both cell types, adavosertib reduced the number of cells in G1 phase significantly. Phendione plus adavosertib decreased the G2/M phase fractions significantly. Phendione increased the numbers of cells in the G1 phase and reduced the G2/M phase population of RS4–11 cells. Adavosertib plus phendione increased G1 phase cells and reduced the S phase cells in RS4–11 cell cultures and reduced G2/M phase populations in both cell types. Both adavosertib and adavosertib plus phendione significantly caused apoptosis-associated DNA fragmentation in MV4–11 and RS4–11 cell cultures (measured as cells with fragmented DNA in subG1 phase) (Fig. 3**F**).

We then applied lower doses of phendione and adavosertib to these cells. In RS4–11 cells, 200 nM phendione plus 200 nM adavosertib promoted apoptosis significantly (supplemental Fig. S1B). An inhibition of WEE1 with 100–200 nM adavosertib ± phendione evoked a significant accumulation of RS4–11 cells in G1 phase (supplemental Fig. S1C).

Immunoblot analyses verified the apoptosis measurements that are shown in Figs. 3**E**,3**F**. We detected cleavage and consequent reduction of the caspase-3 target and DNA repair protein PARP1 in phendione plus adavosertib-treated cells (Fig. 3**G**). This verifies the activation of the ultimate apoptosis executioner enzyme caspase-3. We assessed if this accumulation of apoptosis markers is linked to DNA replication stress/DNA damage. We probed for the phosphorylation of KAP1 at S824, of histone H2AX at S139 (termed γH2AX), and of the DNA replication stress/DNA damage-inducible phosphorylation of the transcription factor p53 at S15. The accumulation of γH2AX corresponded to the extent of apoptosis induction in MV4–11 cells and the accumulation of phosphorylated KAP1 was only evident in the combination scheme. In RS4–11 cells the levels of p-KAP1 correlated with apoptosis but there was no induction of γH2AX. The phosphorylation and levels of p53 were changed hardly by both agents. Detection of the phosphorylation of the WEE1 substrate p-CDK1 revealed the full inhibition of WEE1 by the chosen adavosertib dose in both leukemia cell types (Fig. 3**G**).

These data illustrate that apoptosis induction in leukemia cells is a main consequence of biochemically verified combined inhibition of PP2A and WEE1.

2.4. Phendione and adavosertib kill preleukemic cells, but produce no cytotoxic effects in peripheral blood mononuclear cells (PBMCs)

Next, we evaluated in the HEMAP database if the sensitivities of CML, AML, and ALL cells to PP2A and WEE1 inhibitors are associated with higher expression levels of the mRNAs encoding PP2CA and WEE1

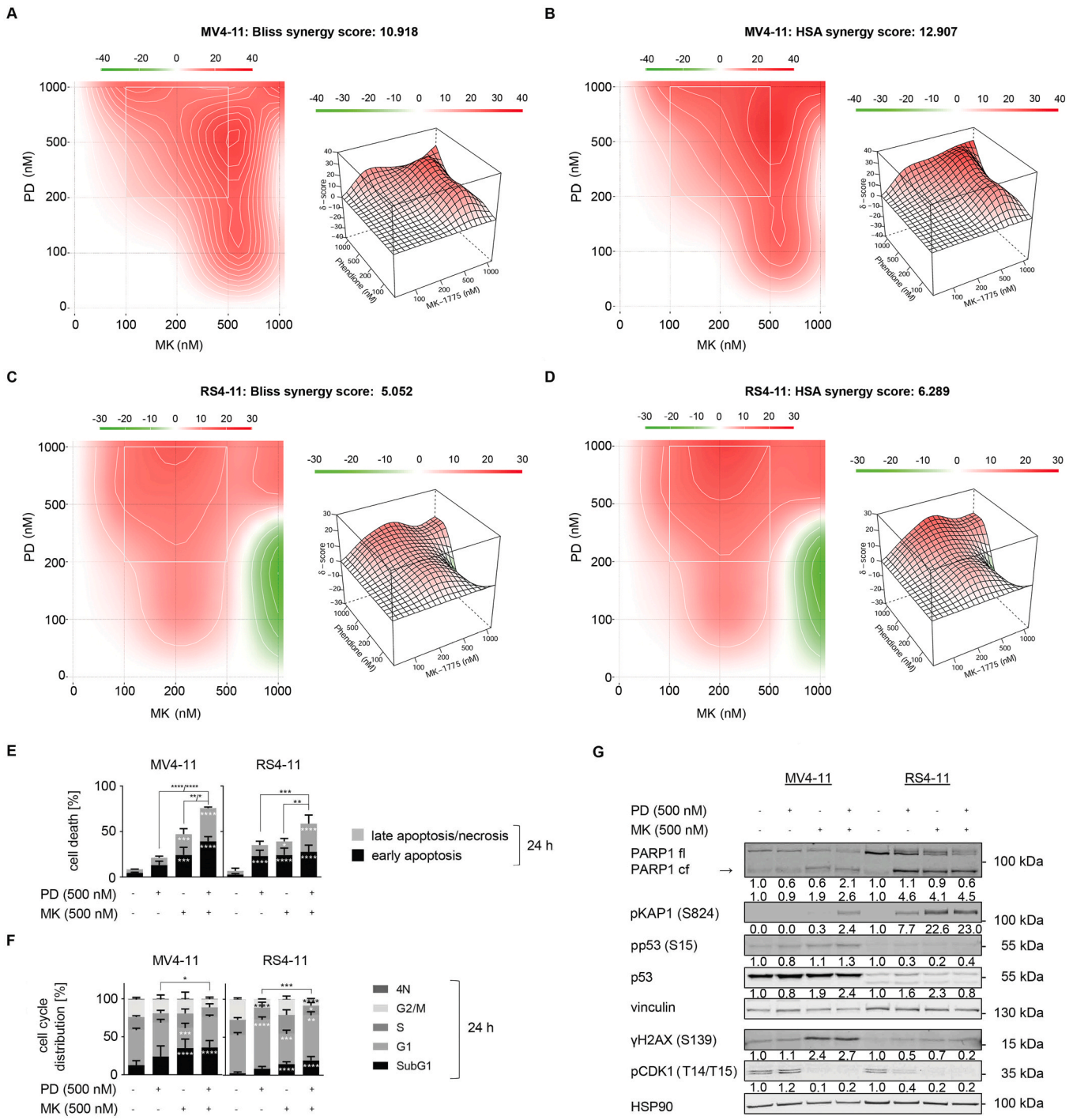

Fig. 3. Phendione and adavosertib synergize to kill leukemic cells. (A-D) Synergy heatmaps visualizing synergistic and antagonistic dose regions in red and green using BLISS and HSA methods, respectively. The white-framed boxes of the maps represent the most synergistic dose combinations. MV4-11 (A,B) and RS4-11 (C,D) cells were treated with the indicated doses of phendione (PD) and adavosertib (MK) for 24 h, harvested, stained with annexin V/PI, and analyzed for cell death by flow cytometry using annexin-V/PI. Synergy scores were analyzed and visualized by the free web-based tool SynergyFinder 3.0 (https://synergyfinder.fimm.fi). (E-F) Cell death determination (E) and cell cycle analysis (F) were performed in MV4-11 and RS4-11 cells. These were treated for 24 h with 500 nM phendione and 500 nM adavosertib. Data are from flow cytometric analyses; n = 3 each; expressed as means ± SD; statistical analyses using analysis of variance (two-way ANOVA; * $p < 0.05$, ** $p < 0.01$, *** $p < 0.001$, **** $p < 0.0001$). (G) Immunoblot was conducted to reveal the levels of the indicated proteins/posttranslational modifications. MV4-11 and RS4-11 cells were treated as mentioned, lysed, and processed; numbers below blots are densitometric values divided by signals for the loading control.

in such cells compared to normal blood cells. There are higher levels of the *PP2CA* and *WEE1* mRNAs in CML and ALL cells than in normal myeloid and T-cells. AML cells had higher levels of WEE1 than myeloid cells (Fig. 4**A**).

To evaluate how phendione might affect normal blood cells, we treated human PBMCs with 0.1–1 μM phendione for 24 h and analyzed individual immune cell fractions. These myeloid and lymphoid leukocyte populations include neutrophils, polymorphonuclear leukocytes (PMNs, granulocytes), dendritic cells (DCs), T-cells, B-cells, and monocytes. A flow cytometry-based determination of cell death showed that phendione did not induce apoptosis in any of these cell types (Fig. 4**B**).

We then tested the effects of 1 μM phendione ± 500 nM adavosertib

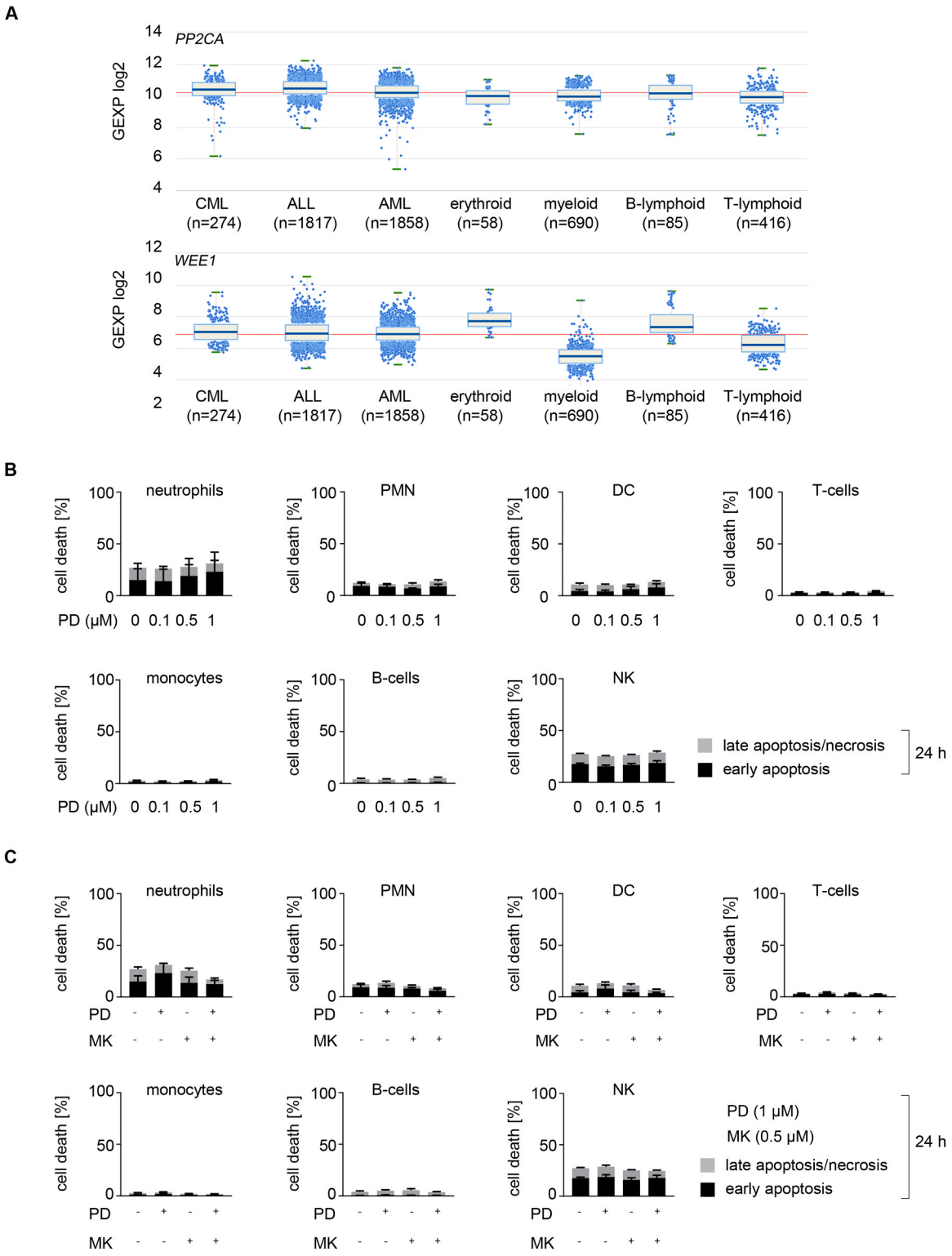

Fig. 4. PP2A and WEE1 inhibitors produce no cytotoxic effects in normal immune cells. (A) The HEMAP database (HEMAP: Blood cancer/AML maps and exploration) was used to detect the mRNA levels encoding PPP2CA and WEE1 in leukemia cells compared to normal cell samples. (B) Neutrophils, PMN, DC, T cells, monocytes, B cells, and NK cells were treated for 24 h with up to 1 μM phendione (PD). (C) These cell types were incubated with 1 μM phendione + 500 nM adavosertib for 24 h (PD/MK). Apoptosis was measured by flow cytometry; n = 4 in each case. All data are mean values ± SD; statistical analyses using analysis of variance (two-way ANOVA) showed no statistical relevance. After harvesting, cells were stained with annexin V-FITC AND SYTOX™ AADvanced™.

for 24 h on PBMCs. Flow cytometry showed that neither adavosertib nor the combination adavosertib + phendione led to an induction of apoptosis in PBMCs (Fig. 4**C**).

These data illustrate that PBMCs are significantly less susceptible to phendione and adavosertib than leukemia cells.

2.5. Phendione and adavosertib kill human and murine PDAC cells

Subsequently, we tried to extrapolate our data to another tumor cell system. We chose PDAC cells for which we have recently characterized their responses to phendione [9]. We inspected the DepMap database for the impact of the genetic depletion of the PP2A catalytic subunits PP2Aα/PP2CA and PP2Aβ/PP2CB and WEE1 in PDAC cells. The proliferation of such cells was compromised by the knockouts of PP2Aα and WEE1 (Fig. 5**A,B**).

Based on our recent findings [9], we incubated human MIA PaCa-2 PDAC cells with 3 μM phendione. We applied 500 nM adavosertib because we had used this concentration to collect the above-shown experimental outcomes with leukemia cells. We evaluated cell cycle progression and apoptosis by flow cytometry. After 24 h, phendione, adavosertib, and their combination reduced the G1 phase populations in MIA PaCa-2 cell cultures significantly. The single treatments augmented the G2/M phase populations, but their combination did not produce this effect. Instead, the combined treatment augmented subG1 phase populations significantly. After 48 h, phendione and adavosertib also increased the subG1 phase fractions significantly and this became more evident in the cotreatment groups. The reduction of G1 phase and the increase in G2/M phase populations by the single agents became significant after 48 h. This was associated with significantly higher numbers of cells in G2/M phase and in case of adavosertib with more cells in S phase. Although phendione plus adavosertib also reduced cells in G1 phase, the accumulation of cells in G2/M phase by the single agents was lost when both agents were applied to MIA PaCa-2 cells (Fig. 5**C**).

Concerning apoptosis induction in MIA PaCa-2 cells, the single agents increased the early apoptotic cell fractions. This became significantly potentiated in the cotreatment scheme after 24 h. After 48 h, these effects were augmented and phendione alone and combined with adavosertib increased the late apoptosis/necrotic fractions significantly (Fig. 5**D**). Immunoblot analysis for cleaved caspase-3 confirmed that phendione plus adavosertib were more effective in inducing apoptosis than the single drug applications (Fig. 5**E**).

To test if phendione acts on target in human PDAC cells, we treated MIA PaCa-2 with 1 μM phendione at early treatment intervals (1 h and 3 h). Like in MV4–11 and RS4–11, we noted a significant accumulation of the PP2A target proteins p-CHK1, p-AKT1, and p-KAP1 prior the onset of detectable apoptosis after a 24-h incubation period (PARP1; annexin-V/PI) or altered proteasomal degradation (PR130) upon PP2A inhibition (Fig. 5**F,G**).

We then investigated whether phendione and adavosertib are effective against the murine PDAC cell line S821, which is weakly susceptible to phendione-induced apoptosis [9]. We treated such cells with 3 μM phendione and 500 nM adavosertib and determined cell death after 48 h and 72 h. Similar to MIA PaCa-2 cells (Fig. 5**C**), the G1 phase was significantly reduced both in the single treatment with phendione or adavosertib and in the combination of phendione plus adavosertib. Adavosertib additionally led to a G2/M arrest. In contrast to the individual treatments, the subG1 fraction increased significantly after 48 h upon the combination treatment. After 72 h, the reduction in G1 phase was maintained in each treatment condition. The single treatments caused no induction of the subG1 fraction even after 72 h, whereas the combination phendione plus adavosertib evoked this apoptosis-associated process significantly (supplemental Fig. S2A). In S821 cells that were treated for 48–72 h, phendione weakly induced apoptosis. Adavosertib induced apoptosis comparably after 48 h and 72 h. The combination of phendione and adavosertib induced apoptosis more effectively than the single treatments. At 72 h, this difference was highly significant for early apoptosis (supplemental Fig. S2B).

From these observations we conclude that inhibitors of PP2A and WEE1 eliminate PDAC cells through apoptosis.

PP2A and WEE1 suppress an accumulation of DNA damage signaling markers and mitotic catastrophe

Next, we investigated whether dysregulation of DNA replication signaling is associated with apoptosis induction by phendione and adavosertib. We treated MIA PaCa-2 cells with 3 μM phendione and 500 nM adavosertib for 24 h. The DNA damage-induced kinase ataxia telangiectasia mutant (ATM) phosphorylates KAP1 to activate KAP1-dependent cell cycle arrest and apoptosis genes [18]. Immunoblots showed an induction of p-KAP1 by phendione alone and more pronouncedly when applied in combination with adavosertib. Treatment with adavosertib also induced p-KAP1 but less effectively than phendione (Fig. 6**A**). As previously reported by us [9], phendione attenuated PR130 after 24 h, but this effect was neither caused nor potentiated by adavosertib (Fig. 6**A**). The PP2A-PR130 complex dephosphorylates activated ATM [19]. The reduction of PR130 by phendione was linked to an accumulation of phosphorylated ATM. Phendione was a stronger inducer of phosphorylated ATM than adavosertib (Fig. 6**A**). This activation of ATM was consistent with the phosphorylation of its target protein KAP1. The accumulation of phosphorylated ATM was not due to its upregulation but associated with ATM species that migrated faster in immunoblot analyses (Fig. 6**A**). These correspond to apoptosis-associated cleavage of ATM by caspases [20].

Due to the alterations in cell cycle progression (Fig. 5**C**) and to ascertain WEE1 inhibitor efficacy in PDAC cells, we probed immunoblots for the cell cycle regulators p-CDK1, its activating binding partner cyclin B, which promotes G2/M phase progression, WEE1, which catalyzes inhibitory phosphorylation of CDK1, and the mitotic serine/threonine kinase polo-like kinase-1 (PLK1). Like in leukemia cells (Fig. 3**G**), adavosertib ceased the phosphorylation of CDK1 in MIA PaCa-2 cells (Fig. 6**B**). Detection of p-CDK1 by immunoblot showed that adavosertib was also an effective inhibitor of WEE1 in S821 cells. A decrease of p-CDK1 and CHK1 was observed in adavosertib and adavosertib plus phendione-treated cells. In addition, an increase of p-KAP1 occurred in such cells (supplemental Fig. S2C). Moreover, adavosertib alone and combined with phendione reduced its target WEE1 together with cyclin B, and PLK1 in MIA PaCa-2 cells (Fig. 6**B**).

Tubulin-α is involved in the proper formation of microtubules for mitosis [21]. Confocal immunofluorescence of MIA PaCa-2 cells demonstrated that adavosertib led to significantly increased star-like tubulin-α structures (Fig. 6**C**), indicating failed mitosis. Typical metaphase cells with normally distributed spindles are visible in untreated MIA PaCa-2 cells. This phenomenon of star-like tubulin-α structures occurred more frequently and significantly in cells that were incubated with adavosertib and phendione. In such cells, we additionally noted an increase in tubulin-α staining intensity and significantly less PLK1 foci, than in MIA PaCa-2 control cells (Fig. 6**C-E**). We could confirm deformed spindle organization, which causes defective mitotic progression, as aberrant acetylated-tubulin (ac-tubulin) staining patterns in MIA PaCa-2 cells that are positive for the G2/M phase marker phosphorylated histone H3 (pH3) (Fig. 6**F,G**). This finding corroborates that phendione plus adavosertib treatment disturbs microtubule dynamics during mitosis.

We deduce that apoptosis induction in PDAC cells that are plated with phendione and adavosertib is linked to mitotic catastrophe.

3. Discussion

The GEPIA2 database shows that high expression levels of both the catalytic PP2A subunit PP2CA and WEE1 tie in with worse prognoses of leukemia patients. Congruently, cultured leukemia cells are killed upon an inhibition of these enzymes. This may also apply to PDAC patients and cells, but we did not analyze the database concerning PDAC samples, because there are issues with PDAC tissues in the TCGA database [22]. Although the number of samples that we analyzed do not allow definite conclusions, our data and database analyses suggest that PP2A is a still underappreciated target in AML and CML.

The dependence of tumor cells on WEE1 can be explained by its critical roles for DNA replication and the timely entry of cells into G2/M

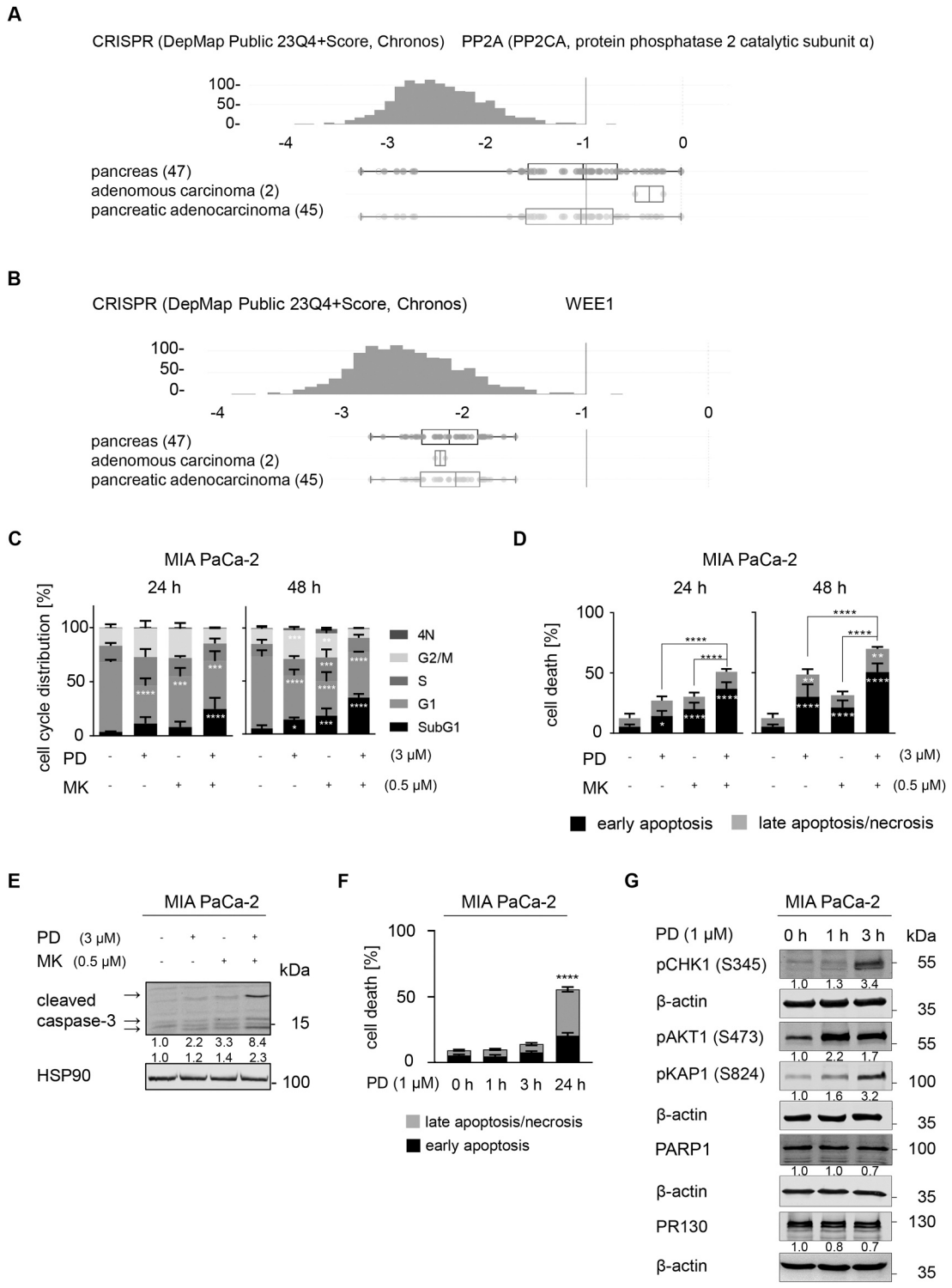

Fig. 5. PP2A and WEE1 are valid targets in PDAC cells. (A,B) The *DepMap* database informs how a CRISPR-Cas9-based depletion of the protein phosphatase 2 catalytic subunit alpha and beta (PPP2CA = PP2Cα) as shown in (A) or WEE1 in (B) are a dependency factors in the indicated tumor cell types. The graph shows the dependency of all analyzed cell types (https://depmap.org/portal/gene). (C) MIA PaCa-2 cells were treated with 3 μM phendione and 500 nM adavosertib for 24–48 h (PD/MK). Cells were fixed and analyzed for cell cycle progression by flow cytometry. (D) Same as in (C), but evaluation of early/late apoptosis/necrosis by flow cytometry for annexin-V/PI. Data from flow cytometric analyses are n = 3 each; expressed as means ± SD; statistical analyses using analysis of variance (two-way ANOVA; * $p < 0.05$, ** $p < 0.01$, *** $p < 0.001$, **** $p < 0.0001$). (E) MIA PaCa-2 cells were treated with 3 μM phendione (PD) and 500 nM adavosertib (MK) for 24 h. Lysates thereof were processed to reveal the activation of caspase-3 by limited proteolysis; HSP90, loading control. (F) MIA PaCa-2 cells were treated with 1 μM for 1 h, 3 h, or 24 h, harvested, stained with annexin V/PI, and analyzed for cell death by flow cytometry. (G) MIA PaCa-2 cells were treated with 1 μM for 1 h and 3 h, harvested, lysed, and immunoblot was performed to detect the levels as well as the posttranslational modifications of indicated proteins. Results represent three independent experiments; numbers are densitometric values divided by signals for the loading control.

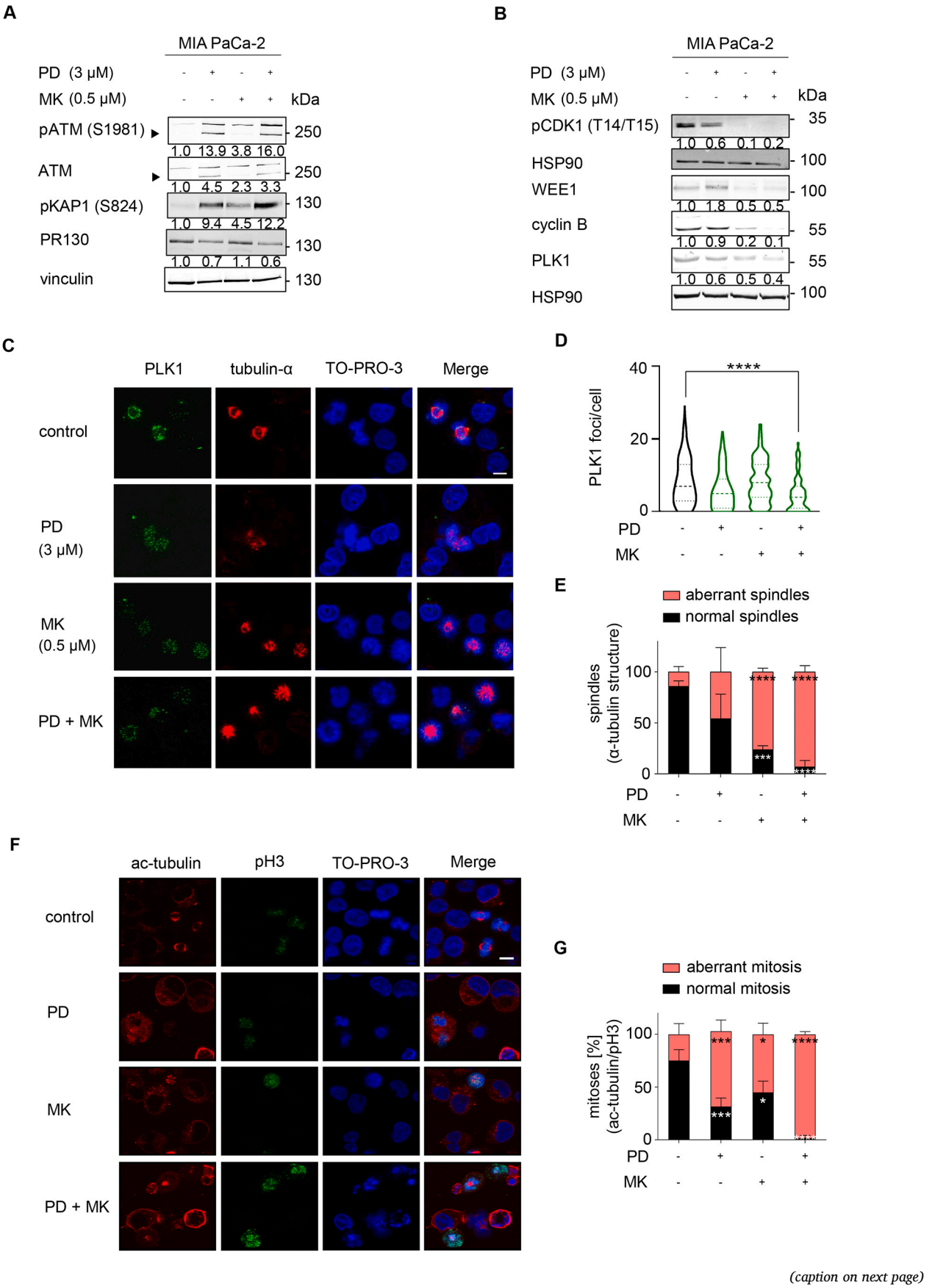

(caption on next page)

Fig. 6. Phendione and adavosertib evoke DNA damage and mitotic catastrophe. (A) MIA PaCa-2 cells were treated with 3 μM phendione (PD) and 500 nM adavosertib (MK) for 24 h. Immunoblots were performed to detect proteins that are activated upon DNA replication stress/DNA damage. Vinculin was detected to control for equal loading; black triangles point to apoptosis-associated cleaved forms (molecular weight of full-length ATM = 350 kDa); n = 2. (B) MIA PaCa-2 cells were treated with 3 μM phendione and 500 nM adavosertib for 24 h (PD/MK). The protein levels of p-CDK1, WEE1, cyclin B, and PLK1 were detected. HSP90 served as loading control; n = 2). Numbers below blots are densitometric values divided by signals for the loading control. (C) MIA PaCa-2 cells were either untreated (control) or treated with 3 μM phendione and 500 nM adavosertib for 24 h, fixed and incubated with anti-a-tubulin or anti-PLK1 antibodies. Antibodies coupled with Alexa Fluor-488 (green, PLK1) and Cy3 (red, tubulin-α) were used for detection. TO-PRO3 was used to visualize the cell nuclei. Representative images are shown; n = 3. PLK1 foci per cell were analyzed using ImageJ software; scale bar 10 μm. (D) Quantification of PLK1 foci in MIA PaCa-2 cells that were treated with 3 μM phendione and 500 nM adavosertib for 24 h. (E) Regular as well as aberrant tubulin-α structures indicating failed deformed spindle organization mitosis/mitotic catastrophe were evaluated in MIA PaCa-2 cells that were exposed to 3 μM phendione and 500 nM adavosertib for 24 h. For D) and E) we analyzed at least 100 cells in three independent experiments. (F) MIA PaCa-2 cells were treated as noted in (C), fixed, and stained with an antibody against the mitotic marker phospho-histone H3 (pH3; Ser10; green) and an antibody against acetylated tubulin (ac-tubulin; Lys40; red). Antibodies coupled with Alexa Fluor-488 and Cy3 were used for detection; TO-PRO3 was used to visualize the cell nuclei. Representative images are shown; n = 3. Normal and deformed ac-tubulin structures in (pH3)-positive (mitotic) cells, indicating normal or failed deformed spindle organization mitosis/mitotic catastrophe were evaluated in MIA PaCa-2 cells. Imaging and analyses were performed in LASX Office software; scale bar 10 μm. The data is expressed as mean ± SD, statistical analyses using analysis of variance (one-way ANOVA) were performed (* $p < 0.05$, *** $p < 0.001$, **** $p < 0.0001$).

phase of the cell cycle [12–14]. Tumor-promoting and tumor-suppressive functions were reported for PP2A [2,7]. Neither clinical data on the patients' prognoses nor data on the reliance of various tumor cells on PP2A support major tumor-suppressive functions of PP2A. PP2A rather appears as a valid clinical target in AML, CML, and PDAC cells. This notion reflects recent data and the above data, which demonstrate that PP2A inhibition eliminates cancer cells in culture and in mice [6,8,9].

Adavosertib is used in advanced clinical trials [15,16]. Inhibitors for PP2A and WEE1 may be improved by pharmaceutical approaches, including but not limited to the development of targeted protein degraders of WEE1 and PP2A based on existing inhibitors [23,24]. Treating leukemia cells and PDAC cells with phendione plus adavosertib evokes in a synergistic range over various concentrations apoptosis, a loss of cells in G2/M phase, biochemical signs of DNA replication stress/DNA damage, and mitotic catastrophe. Further studies are necessary to clarify the exact DNA damage and DNA repair pathways in cells with blocked PP2A and WEE1, and if these pathways include therapeutic targets to kill cancer cells.

If WEE1 is active, CDK1 is phosphorylated and therefore inactive and cells do not enter G2/M phase prematurely [12–14]. We observed an increase in tubulin-α staining intensity and the accumulation of aberrant tubulin-α staining patterns in adavosertib plus phendione-treated cells, despite reduced cell numbers in G2/M phase and despite an accumulation of DNA replication stress marker proteins. Such cellular alterations indicate mitotic catastrophe [25]. PLK1 signaling controls the assembly of the spindle apparatus that separates the duplicated chromosomes in G2 phase and the progression of mitosis. These activities of PLK1 maintain genomic integrity and prevent apoptosis [26]. Our finding that mitotic catastrophe results in caspase-3 activation suggests that apoptosis induction is associated and probably results from such mitotic defects.

Taken together, this work shows that leukemia cells from ALL and CML patients and PDAC cells undergo mitotic defects and apoptosis upon treatment with phendione and adavosertib. Although our data is limited to the use of cell lines and primary cells ex vivo, we provide a possible framework for improved therapy of patients suffering from these and further severe tumors.

3.1. Material and methods

3.1.1. Drugs and chemicals

Adavosertib was purchased from Selleck Chemicals, Munich, Germany. Phendione (1,10-phenanthroline-5,6-dione), propidium iodide (PI), and triton X-100 were purchased from Sigma-Aldrich Chemie GmbH, Munich, Germany; dithiothreitol (DTT) was from PanReac AppliChem, Darmstadt, Germany; and bovine milk powder were from Carl Roth, Karlsruhe, Germany. All drugs were kept as stock solutions in DMSO at −80°C.

3.1.2. Cells and culture conditions

HEL, erythroleukemia (AML M6), relapse after Hodgkin-lymphoma, 30-year-old male, $JAK2^{V617F}$-Mutation, p53-mutant, p16-mutant; K562, CML crisis, 53-year-old female, p53-negative; MV4–11, AML, 10-year-old boy, FLT3-ITD, MLL-AFF1/MLL-AF4; Ramos, Burkitt-lymphoma, 3-year-old boy, MYC overexpression; RS4–11, B-cell precursor leukemia, ALL, 32-year-old female, p53-mutant, MLL-AFF1/MLL-AF4; MIA PaCa-2, human PDAC cell line, isolated from a 65-year-old Caucasian man in 1975, KRAS-mutant, p53-mutant, p16-deletion; S821 murine PDAC cell line isolated from a primary pancreatic tumor, KRAS-mutant, p16-Deletion, p53-mutant [27]. Leukemic cells were cultured in Roswell Park Memorial Institute-1640 (RPMI-1640) (Sigma-Aldrich, Steinheim, Germany) supplemented with 5–10% fetal bovine serum (FCS) (Sigma-Aldrich, Steinheim, Germany), 1% penicillin/streptomycin (Sigma-Aldrich, Steinheim, Germany). Adherent cell lines were maintained in Dulbecco's Modified Eagle Medium (DMEM), 5–10% FCS (Sigma-Aldrich, Steinheim, Germany), 1% penicillin/streptomycin (Life Technologies, USA). All cells were maintained under standard sterile conditions in humidified, 5% CO_2 atmosphere at 37°C. All cell lines were tested negative for mycoplasma. Human cells were authenticated by DNA fingerprint at the DSMZ, Braunschweig or Eurofins Genomics, Ebersberg, Germany.

3.1.3. MLL-ENL+ pre-leukemic cells and primary CML cells

To establish a primary human AML *in vitro* model, human CD34 + cells from healthy donors were retrovirally transduced with the t(11;19) *MLL-ENL* (ME) fusion gene. The outgrowth of MLL-ENL+ cells was monitored by the increase of GFP+ cells. Fully outgrown MLL-ENL+ cells were seeded at 3×10^5 cells/mL in complete medium (IMDM medium supplemented with 20% FCS, 100 U/mL penicillin/streptomycin, 2 mM L-glutamine, 20 ng/mL FLT3 ligand, 20 ng/mL GM-CSF, 20 ng/mL SCF, 20 ng/mL TPO, 20 ng/mL IL-6, and 10 ng/mL IL-3). Primary CML cells were described by us [28]. In brief, mononuclear cells were isolated upon approval of the Ethical Committee of Landesärztekammer Rhineland-Palatine No.: 837.258.17 (11092) from a 39-year-old female with the BCR-ABL transcript b2a2 and suffering from chronic phase t(9;22)-positive CML. Cells were collected by Ficoll Hypaque gradient and cultivated in L-glutamine containing Iscove's Modified Dulbecco's Medium (IMDM) (Thermo Fisher Scientific, Darmstadt, Germany) supplemented with 20% fetal bovine serum, 1% penicillin/streptomycin, 1x MEM non-essential amino acids (Euro-Clone), 10 ng/mL Interleukin-3, and 50 ng/mL FLT3 ligand (Pepro-Tech/Thermo Fisher Scientific, Darmstadt, Germany). All cells were maintained under sterile conditions at 37°C in a humidified incubator with 5% CO_2.

3.1.4. PBMCs

We have recently described this technique in [29]. PBMCs were isolated with Biocoll® separation solution from buffy coats. These were

from four healthy donors who were tested negative for general infections. As mentioned in [29], PBMCs were washed in staining buffer (1x PBS, 2% FCS, 0.5 mM EDTA) and incubated with human FcR blocking reagent (No. 130–059–901, Miltenyi Biotec) to prevent antibody binding to Fc receptors. The samples were then incubated with fluorescently labeled antibodies (20 min, 4 °C) and washed with 1x PBS. Subsequently, staining with Annexin-V FITC (640906, BioLegend) was performed for 20 min in the absence of light to determine early apoptosis. To detect the cells in late apoptosis/necrosis, the dye SYTOX™ AADvanced™ (S10349) was added to the samples 5 min prior to measurements. Measurements and analyses were performed using the AttuneTM NxT flow cytometer and the Attune NxT software (Thermo Fisher). The cells were defined: CD3+ as T cells, CD3- CD19+ as B cells, CD3- CD19- CD14+ as monocytes, CD3- CD19- CD1c+ as dendritic cells, CD3- CD19- CD56+ as natural killer (NK) cells, CD3- CD14- CD19- CD56- CD11b+ CD15+ as neutrophils, and CD3- CD14- CD19- CD56- CD11b+ as PMNs. The following antibodies were used: CD11b BV510 (101263), CD1c BV605 (331538), CD3 BV711 (344838), CD14 PE (301850) from BioLegend; CD15 APC (17–0158–42), CD56 PE-Cy7 (25–0567–42), CD19 SuperBright436 (62–0199–42); all from Thermo Fisher.

3.1.5. Immunoblot

Cells were harvested, lysed in NET-N buffer (100 mM NaCl, 10 mM Tris-HCl pH 8, 1 mM EDTA, 10% glycerol, 0.5% NP-40; protease inhibitor cocktail tablets (Roche, Mannheim, Germany) and phosphatase inhibitor cocktail 2 (Sigma)), sonicated (20 pulses, amplitude 40%, 0.1 s pulse duration) and centrifuged (17,000 ×g/25 min/4 °C). Protein concentrations were estimated by Bradford assay. Proteins were analyzed by SDS-PAGE (95–125 V for 90 min) and immunoblot (175 mA per gel for 120 min). After transfer onto nitrocellulose membranes (Amersham Protran, GEHealthcare), membranes were blocked with 5% non-fat milk for 1 h, washed in Tris-buffered saline/Tween (TBS-T) for 5 min each, and incubated overnight with the following primary antibodies: p-ATM (Ser1981)/ab-81292, p21/ab-109199 (Abcam, Cambridge, UK), ATM/cs-2873, CHK1/cs-2360, cleaved caspase-3/cs-9661, cyclin B1/cs-4138, p-AKT (Ser473)/cs-9271S, p-CDK1 (Tyr15)/cs-4539S, p-CHK1 (S345)/cs-2348S, p-p38 (Thr180/Tyr182)/cs-9215, WEE1/cs-4936, ɣH2AX (Ser139)/cs-9718 (Cell Signaling, Frankfurt/Main); cleaved PARP1/552596, PARP1/556362 (BD Bioscience, Heidelberg); β-actin/sc-47778, HSP90/sc-13119, p53-DO1/sc-126, vinculin (7F9), sc-73614 (Santa Cruz, Heidelberg); p53/NCL-p53-CM5p (Novocastra Leica Biosystems, Wetzlar); p-KAP1 (Ser824), PR130/NBP1–87233 (Novus Biologicals, Wiesbaden). Membranes were afterwards incubated with secondary antibodies as follows: IRDye® 680RD anti-rabbit IgG/925–68071, IRDye® 680RD anti-mouse IgG/925–68070, IRDye® 800CW anti-rabbit IgG/925–32211, IRDye® 800CW anti-mouse IgG, 925–32210 (LI-COR Biosciences, Bad Homburg); Alexa Fluor® 488 F(ab'2) anti-mouse IgG (H+L)/A11017 (Thermo Fischer, Frankfurt/Main); Cy3 anti-rabbit IgG (H+L)/111–165–144 (Dianova, Hamburg). Proteins were analyzed using the Infrared Imaging System Odyssey (LICOR). Data analysis was performed using Image Studio Lite V4.0 (LICOR).

3.1.6. Flow cytometry

Annexin/PI staining: the samples were centrifuged for 5 min at 1300 rpm and room temperature. Cell pellets were washed twice with 1 mL PBS. Afterwards, cells were stained with 2.5 μL annexin-V-FITC (Miltenyi Biotec) and 50 μL 1x binding buffer (1 mM HEPES, 140 mM NaCl, 0.25 mM $CaCl_2$, pH was adjusted to 7.4 with KOH) for 20 min in darkness. Shortly before measurement, cells were stained with 10 μL PI (50 μg/mL) and 430 μL 1x binding buffer and measured with the BD FACS Canto II. Data analysis was carried out using FACSDiva Software (BD Biosciences). Cells in late apoptosis or necrotic cells show both annexin V and PI-positive staining, as the integrity of the plasma and nuclear membrane decreases, allowing PI to enter the cell, intercalate into the DNA and emit fluorescence in the flow cytometer. Cells undergoing early events of apoptosis are negative for PI staining.

Analysis of cell cycle phases and subG1 fractions: cells were harvested and washed twice with 1x PBS and fixed with 2 mL ice-cold 80% EtOH for 2 h. On the day of measurement, the samples were centrifuged for 5 min at 1300 rpm. The supernatant was aspirated, and the pellets were washed with 1x PBS. The pellets were resuspended in 333 μL 1x PBS and 1 μL RNase A (10 mg/mL) and incubated for 1 h at room temperature. Shortly before the measurement, 165 μL PI (50 μg/mL) were added to the samples. Cellular debris were out-gated. Intensity of PI fluorescence signal was measured with the FACSCanto II flow cytometry machine (BD Biosciences) and analyzed using FACSDiva Software.

3.1.7. Synergy assessment

Synergy between drug pairs was quantified and visualized using the web-based SynergyFinder 3.0 platform [30], based on apoptosis measurements. Early and late apoptotic values were summed up and normalized to control values. This prompt dose-response matrices for each combination and computed synergy scores across the matrix based on standard reference models (BLISS and HSA). For each dose combination, the observed effect was compared to the model-predicted non-interaction effect to obtain a local synergy score, and these values were then summarized into an overall synergy score for the full matrix to reduce model-specific false positives. Zero, > 0 or < 0 corresponds to additive, synergy or antagonism, respectively, whilst > 5 indicates strong synergy [31].

3.1.8. Immunofluorescence

Immunofluorescence was performed using anti-PLK1/sc-17783 (Santa Cruz, Heidelberg) and anti-α-tubulin/ab-6560 (Abcam, Cambridge, UK), anti-ac-tubulin (Lys40)/T7451 (Sigma-Aldrich, Darmstadt, Germany), and anti-p-H3 (Ser10)/cs-9701S (Cell Signaling, Frankfurt/Main), as previously described by us [9,17]. Imaging and data analysis were carried out using the laser-scanning microscope LSM710 with Zen 2009 software (Carl Zeiss) or the Leica TCS SP8 inverse confocal fluorescence microscope using LASX Office software. The scoring rubric for aberrant mitoses includes cells with multipolar spindles, star-shaped microtubules, dispersed acetylated tubulin, failed cytokinesis, and scattered nuclear morphology. At least ≥ 200 cells per condition were analyzed by us unblinded and from three independent biological replicates.

3.1.9. Database analyses

We used the databases GEPIA2 (GEPIA 2), UALCAN (https://ualcan.path.uab.edu/analysis.html): an update to the integrated cancer data analysis platform that contains information from the TCGA, MET500, CPTAC and CBTTC, and GTEx databases, DepMap (DepMap: The Cancer Dependency Map Project at Broad Institute), and HEMAP (http://hemap.uta.fi/hemap/index.html).

CRediT authorship contribution statement

Oliver Holger Krämer: Writing – review & editing, Writing – original draft, Visualization, Supervision, Software, Resources, Project administration, Funding acquisition, Data curation, Conceptualization. **Christian Wichmann:** Supervision, Resources, Methodology. **Linping Chen-Wichmann:** Supervision, Resources, Methodology. **Stefan Stoldt:** Formal analysis, Methodology, Resources, Software. **Walburgis Brenner:** Validation, Resources. **Yesim Melisa Gürbüzoglu:** Formal analysis, Investigation, Validation. **Markus P. Radsak:** Validation, Resources. **Matthias Bros:** Validation, Supervision, Resources, Conceptualization. **Yanira Zeyn:** Visualization, Investigation, Formal analysis. **Sophie Kreissig:** Visualization, Investigation, Formal analysis. **Alexandra Nguyen:** Writing – original draft, Visualization, Methodology, Investigation, Formal analysis. **Al-Hassan M. Mustafa:** Writing – review

& editing, Writing – original draft, Visualization, Validation, Supervision, Methodology, Investigation, Formal analysis, Conceptualization.

Funding

Work done in the group of OHK is funded by the Deutsche José Carreras Leukämie-Stiftung (José Carreras Leukemia Foundation, Projekt DJCLS 09 R/204); the H.W. & J. Hector Stiftung, project M 2419; the German Research Foundation/Deutsche Forschungsgemeinschaft (DFG) KR2291/12–2, DFG-project number 445785155; KR2291/18–1, project number 528202295; DFG KR2291/14–1, project number 469954457; KR2291/15–1, project number 495271833; KR2291/16–1, project number 496927074; KR2291/17–1, project number 502534123; Project-ID 393547839 – SFB 1361; the DAAD Egypt/Germany; the Brigitte und Dr. Konstanze Wegener-Stiftung (project 110); the Walter Schulz-Stiftung; the Dr. Werner Jackstädt-Stiftung; MPR acknowledges funding from Project-ID 318346496 - SFB1292 TP21N.

Declaration of Competing Interest

OHK declares the patents “The use of molecular markers for the preclinical and clinical profiling of inhibitors of enzymes having histone deacetylase activity, WO/2004/027418”, “Novel HDAC6 inhibitors and their uses, WO2016020369A1”, and “Synthesis, pharmacology and use of new and selective FMS-like tyrosine kinase 3 (FLT3) inhibitors, WO2019/034538”, and advisory consultant activity for BASF, Ludwigshafen, Germany. The substances that are covered in these patents are not those that are shown in the submitted manuscript. Thus, there are no direct competing interests. All other authors declare that they have no conflict of interest.

Acknowledgement

We thank Christina Brachetti and Robert Prause for their excellent technical assistance.

Appendix A. Supporting information

Supplementary data associated with this article can be found in the online version at doi:10.1016/j.biopha.2026.119433.

Data availability

Data will be made available on request.

References

[1] D. Hanahan, Hallmarks of cancer: new dimensions, Cancer Discov. 12 (2022) 31–46.
[2] H. Nguyen, A.N. Kettenbach, Substrate and phosphorylation site selection by phosphoprotein phosphatases, Trends Biochem Sci. 48 (2023) 713–725.
[3] M. Dzulko, M. Pons, A. Henke, G. Schneider, O.H. Krämer, The PP2A subunit PR130 is a key regulator of cell development and oncogenic transformation, Biochim Biophys. Acta Rev. Cancer 1874 (2020) 188453.
[4] T.J. Haanen, C.M. O'Connor, G. Narla, Biased holoenzyme assembly of Protein Phosphatase 2A (PP2A): from cancer to small molecules, J. Biol. Chem. 298 (2022).
[5] H. Ronk, J.S. Rosenblum, T. Kung, Z. Zhuang, Targeting PP2A for cancer therapeutic modulation, Cancer Biol. Med. 19 (2022) 1428–1439.
[6] M.H. Dias, A. Friskes, S. Wang, J.M. Fernandes Neto, F. van Gemert, S. Mourragui, C. Papagianni, H.J. Kuiken, S. Mainardi, D. Alvarez-Villanueva, C. Lieftink, B. Morris, A. Dekker, E. van Dijk, L.H.S. Wilms, M.S. da Silva, R.A. Jansen, A. Mulero-Sanchez, E. Malzer, A. Vidal, C. Santos, R. Salazar, R.A.M. Wailemann, T.E.P. Torres, G. De Conti, J.A. Raaijmakers, P. Snaebjornsson, S. Yuan, W. Qin, J. S. Kovach, H.A. Armelin, H. Te Riele, A. van Oudenaarden, H. Jin, R. L. Beijersbergen, A. Villanueva, R.H. Medema, R. Bernards, Paradoxical activation of oncogenic signaling as a cancer treatment strategy, Cancer Discov. 14 (2024) 1276–1301.
[7] S. Reynhout, V. Janssens, Physiologic functions of PP2A: lessons from genetically modified mice, Biochimica Et Biophysica Acta (BBA)-Molecular Cell Research 1866 (2019) 31–50.
[8] J. Yue, R. Vendramin, F. Liu, O. Lopez, M.G. Valencia, H.G. Dos Santos, G. Gaidosh, F. Beckedorff, E. Blumenthal, L. Speroni, Targeted chemotherapy overcomes drug resistance in melanoma, Genes Dev. 34 (2020) 637–649.
[9] A. Nguyen, A.M. Mustafa, A.K. Leydecker, M. Halilovic, J. Murr, F. Butter, O. H. Krämer, The protein phosphatase-2A subunit PR130 is involved in the formation of cytotoxic protein aggregates in pancreatic ductal adenocarcinoma cells, Cell Commun. Signal 22 (2024) 217.
[10] V. Chung, A.S. Mansfield, F. Braiteh, D. Richards, H. Durivage, R.S. Ungerleider, F. Johnson, J.S. Kovach, Safety, tolerability, and preliminary activity of LB-100, an inhibitor of protein phosphatase 2A, in Patients with Relapsed Solid Tumors: an open-label, dose escalation, first-in-human, phase i trial, Clin. Cancer Res. 23 (2017) 3277–3284.
[11] H. Ronk, J.S. Rosenblum, T. Kung, Z. Zhuang, Targeting PP2A for cancer therapeutic modulation, Cancer Biol. Med. 19 (2022) 1428–1439.
[12] A. Ghelli Luserna di Rora, C. Cerchione, G. Martinelli, G. Simonetti, A WEE1 family business: regulation of mitosis, cancer progression, and therapeutic target, J. Hematol. Oncol. 13 (2020) 126.
[13] K. Mahajan, N.P. Mahajan, WEE1 tyrosine kinase, a novel epigenetic modifier, Trends Genet 29 (2013) 394–402.
[14] N.Y.L. Ngoi, M.M. Pham, D.S.P. Tan, T.A. Yap, Targeting the replication stress response through synthetic lethal strategies in cancer medicine, Trends Cancer 7 (2021) 930–957.
[15] A. Kong, H. Mehanna, WEE1 inhibitor: clinical development, Curr. Oncol. Rep. 23 (2021) 107.
[16] C. Zhang, K. Peng, Q. Liu, Q. Huang, T. Liu, Adavosertib and beyond: biomarkers, drug combination and toxicity of WEE1 inhibitors, Crit. Rev. Oncol. Hematol. 193 (2024) 104233.
[17] C. Hieber, A.M. Mustafa, S. Neuroth, S. Henninger, H.P. Wollscheid, J. Zabkiewicz, M. Lazenby, C. Alvares, S. Mahboobi, F. Butter, W. Brenner, M. Bros, O.H. Krämer, Inhibitors of the tyrosine kinases FMS-like tyrosine kinase-3 and WEE1 induce apoptosis and DNA damage synergistically in acute myeloid leukemia cells, Biomed. Pharm. 177 (2024) 117076.
[18] S. Iyengar, P.J. Farnham, KAP1 protein: an enigmatic master regulator of the genome, J. Biol. Chem. 286 (2011) 26267–26276.
[19] A. Göder, C. Emmerich, T. Nikolova, N. Kiweler, M. Schreiber, T. Kühl, D. Imhof, M. Christmann, T. Heinzel, G. Schneider, O.H. Krämer, HDAC1 and HDAC2 integrate checkpoint kinase phosphorylation and cell fate through the phosphatase-2A subunit PR130, Nat. Commun. 9 (2018) 764.
[20] A. Nguyen, M. Dzulko, J. Murr, Y. Yen, G. Schneider, O.H. Krämer, Class 1 histone deacetylases and ataxia-telangiectasia mutated kinase control the survival of murine pancreatic cancer cells upon dNTP depletion, Cells 10 (2021).
[21] L.T. Ferreira, A.C. Figueiredo, B. Orr, D. Lopes, H. Maiato, Dissecting the role of the tubulin code in mitosis, Methods Cell Biol. 144 (2018) 33–74.
[22] I. Peran, S. Madhavan, S.W. Byers, M.D. McCoy, Curation of the pancreatic ductal adenocarcinoma subset of the cancer genome atlas is essential for accurate conclusions about survival-related molecular mechanisms, Clin. Cancer Res. 24 (2018) 3813–3819.
[23] V.J. Alli, P. Yadav, V. Suresh, S.S. Jadav, Synthetic and medicinal chemistry approaches toward WEE1 kinase inhibitors and its degraders, ACS Omega 8 (2023) 20196–20233.
[24] P.H. Chen, Z. Hu, E. An, I. Okeke, S. Zheng, X. Luo, A. Gong, S. Jaime-Figueroa, C. M. Crews, Modulation of phosphoprotein activity by phosphorylation targeting chimeras (PhosTACs), ACS Chem. Biol. 16 (2021) 2808–2815.
[25] M.M. Mc Gee, Targeting the mitotic catastrophe signaling pathway in cancer, Mediat. Inflamm. 2015 (2015) 146282.
[26] I. Shakeel, N. Basheer, G.M. Hasan, M. Afzal, M.I. Hassan, Polo-like Kinase 1 as an emerging drug target: structure, function and therapeutic implications, J. Drug Target 29 (2021) 168–184.
[27] S. Mueller, T. Engleitner, R. Maresch, M. Zukowska, S. Lange, T. Kaltenbacher, B. Konukiewitz, R. Ollinger, M. Zwiebel, A. Strong, H.Y. Yen, R. Banerjee, S. Louzada, B. Fu, B. Seidler, J. Gotzfried, K. Schuck, Z. Hassan, A. Arbeiter, N. Schonhuber, S. Klein, C. Veltkamp, M. Friedrich, L. Rad, M. Barenboim, C. Ziegenhain, J. Hess, O.M. Dovey, S. Eser, S. Parekh, F. Constantino-Casas, J. de la Rosa, M.I. Sierra, M. Fraga, J. Mayerle, G. Kloppel, J. Cadinanos, P. Liu, G. Vassiliou, W. Weichert, K. Steiger, W. Enard, R.M. Schmid, F. Yang, K. Unger, G. Schneider, I. Varela, A. Bradley, D. Saur, R. Rad, Evolutionary routes and KRAS dosage define pancreatic cancer phenotypes, Nature 554 (2018) 62–68.
[28] A.G. Kansy, R. Ashry, A.M. Mustafa, A.M. Alfayomy, M.P. Radsak, Y. Zeyn, M. Bros, W. Sippl, O.H. Krämer, Pharmacological degradation of ATR induces antiproliferative DNA replication stress in leukemic cells, Mol. Oncol. (2024).
[29] Y. Zeyn, K. Hausmann, M. Halilovic, M. Beyer, H.S. Ibrahim, W. Brenner, S. Mahboobi, M. Bros, W. Sippl, O.H. Krämer, Histone deacetylase inhibitors modulate hormesis in leukemic cells with mutant FMS-like tyrosine kinase-3, Leukemia 37 (2023) 2319–2323.
[30] A. Ianevski, A.K. Giri, T. Aittokallio, SynergyFinder 3.0: an interactive analysis and consensus interpretation of multi-drug synergies across multiple samples, Nucleic Acids Res. 50 (2022) W739–W743.
[31] P. Makela, S.M. Zhang, S.G. Rudd, Drug synergy scoring using minimal dose response matrices, BMC Res. Notes 14 (2021) 27.